

Research Paper

Black Phosphorus Mid-Infrared Photodetector with Circular Au/Pd Antennas

Somaye Jalaei¹, Javad Karamdel*¹, Hassan Ghalami-Bavil-Olyae²

¹ Department of Electrical Engineering, South Tehran Branch, Islamic Azad University, Tehran, Iran

² Department of Physics, South Tehran Branch, Islamic Azad University, Tehran, Iran

Received: 11 Dec. 2021

Revised: 25 Jan. 2022

Accepted: 23 Feb. 2022

Published: 5 Mar. 2022

Use your device to scan
and read the article online



Keywords:

Bandgap, Black Phosphorus, Medium Wavelength

Abstract: Black phosphorus has been considered as one of the most capable two-dimensional materials for use in optoelectronic nanodevices due to its intrinsic layered nature structure, high mobility of carrier, and tunable bandgap. But its low light absorption prevents its use in high-efficiency photodetectors. In this study, the circular Au/Pd antenna-assisted black phosphorus mid-infrared photodetector which significantly improves the detection performance in comparison with BP photodetectors without antenna has been proposed. By integrating a circular Au/Pd antenna on the BP surface, the light-BP interaction was significantly increased. The simulation results demonstrate that metallic antenna structures improve both light absorption and photocarrier collection in BP phosphorus detectors. The numerical result shows that the photocurrent of the mid-infrared antenna-assisted BP detector was 5 times larger than that of BP photodetector without antennas.

Citation: Jalaei S, Karamdel J, Ghalami Bavil Olyae H. Black Phosphorus Mid-Infrared Photodetector with Circular Au/Pd Antennas.

Journal of Optoelectrical Nanostructures, 2022; 7 (1): 37-54

DOI: [10.30495/JOPN.2022.29104.1239](https://doi.org/10.30495/JOPN.2022.29104.1239)

***Corresponding author:** Javad Karamdel

Address: Department of Electrical Engineering, South Tehran Branch, Islamic Azad University, Tehran, 1777613151, Iran. **Tell:** 00989390179135

Email: j-karamdel@azad.ac.ir

1. INTRODUCTION

Recently, BP has transpired as an attractive material for optoelectronic and electronic usages owing to its adjustable bandgap from 0.3 eV (bulk) to 2 eV (monolayer) and unexpected high mobility of carrier [1-4]. Moreover, the bandgap of BP is extremely tunable by varying the number of layers [5-8]. Therefore, BP can be used for the realization of photodetection from visible to infrared wavelengths. A Comprehensive review of the photodetectors based on BP covering the detection spectrum from ultraviolet to infrared has been reported by Long et al [9]. A small bandgap of a few layers BP is an appropriate applicant for the detection of mid-IR photons [10-13].

Comprehensive theoretical and experimental investigations in recent led to the fabrication of photodetectors based on BP in the mid-IR span [14-18]. The successful fabrication of BP-based photodetector with a channel thickness of 10nm working at 3.39 μm leading to the high responsivity of 82A.W^{-1} has been done in early 2016 [19]. In another work, Mei and Yuqian studied BP photodetector which can detect wavelength ranges from 2.5 to 3.7 μm [20]. Furthermore, the broadband photodetection in the Mid-Wave infrared region has been efficaciously illustrated in different heterostructures consisting of BP [21-23]. Many endeavors have been done to further improvement of the performance of photodetectors based on BP in terms of photon absorption efficiency and responsivity that operates from UV to IR ranges [24]. In particular, a BP-based photodetector with high efficiency was reported by Wu et al that operates at UV range with a responsivity of 10^4A.W^{-1} [25].

Lately, Huang et al. demonstrated a high-performance broadband BP photodetector which presented an excellent responsivity of $4.3 \times 10^6\text{A.W}^{-1}$ at 633nm [26]. In another research, Kochar et al. represented MoS₂/P heterostructure to achieve a good rate of absorption in the visible spectral region [27]. However, it is noteworthy that enhancing the optical absorption of BP in the important mid-IR regime is still lower than expected.

Yet, considerable attempts have been expended to make better the light absorption of BP. For example, Qing et al. suggested an adjustable absorber based on BP composed of BP monolayer, a metallic mirror, and photonic crystal to improve absorption of the light at terahertz radiation [28]. Dong et al. designed a Near-infrared absorber consisting of a metal film, a separator with an inner monolayer BP, and a distributed Bragg reflector, which ensues in a maximum absorption improvement of around 100% [29]. In addition, Liu et al.

suggested a simple structure with high-efficiency absorption in the mid-IR which is fabricated from BP which is sandwiched with dielectric materials with low index contrast and polymer [30]. Similarly, Audhkhasi and Povinelli proposed a gold nanostructured design to achieve enhanced absorption in the thin BP films in the 3–5 μm wavelength range [31]. Also, Sefidmooye et al. enhance the light-matter interaction in 2D materials and photodetection performance by using an optical cavity substrate [32].

Increasing the lifetime of the carrier by providing a carrier trapping process can increase the light absorption of materials and enhance the optical responsivity of the photodetector. Of course, this method also increases the response time of the photodetector by a few seconds [33-35]. An alternative approach to getting great responsivity without increasing the response time of the detector is to enhance the photocarrier group performance with a short carrier lifetime [36].

In this paper, we demonstrate a circular antenna-assisted BP detector design for the mid-IR range and increase absorption of light and carrier collection performance with these optical antennas. Comparative studies on the optical characterization of BP photodetector with antenna and without antenna have been accomplished through the finite difference time domain. In addition, the electrical characterization of BP photodetector ($I_d - V_g$ and $I_d - V_d$) under illuminated and dark conditions have been performed separately. Compared to BP-based optical detectors without antenna, our proposed photodetector illustrates well performance in the terms of photocurrent and responsivity at $\lambda = 4\mu\text{m}$. The responsivity of the proposed photodetector reaches up to 6.25A.W^{-1} at a light power of 400mWcm^{-2} with small source-drain bias ($V_{ds} = 100\text{mV}$).

2. WORKING METHOD

The computer analysis of the antenna-assisted BP mid-IR photodetector is simulated in numerical DEVICE/FDTD. First, we study optical characterization via the FDTD module. Then to determine the electrical characterization, the total generation rate is imported into the DEVICE. Further, the electrical characterization of the proposed structure is studied with DEVICE charge solver software.

A. Theoretical Methodologies and Computational Details

The absorption per unit volume of the proposed structure in the FDTD solution is calculated through this equation [37]:

$$P_{abs} = -0.5\omega |E|^2 \text{image}(\epsilon) \quad (1)$$

Where ω , E and ϵ are the angular frequency, the electric field, and the permittivity respectively.

By dividing P_{abs} with the unit energy of the photon $\hbar\omega$, the number of photons absorbed per unit area is obtained. Next by integrating g over the simulation spectrum, the total generation rate is also computed [38]:

$$g = \frac{P_{abs}}{\hbar\omega} \quad (2)$$

Under monochromatic illuminations of photon energy, the photo-generated electrons and holes move in response to bias voltage and photocurrent (I_{ph}) was obtained [39-42]:

$$I_{ph} = I_{light} - I_{dark} \quad (3)$$

The responsivity is the ratio of the output photocurrent to the power of the incident light and it is an important key parameter to evaluate the performance of photodetectors [43]:

$$R(A \times W^{-1}) \equiv \frac{I_{ph}}{P_{in}} \equiv \frac{I_{ph}}{\Phi \hbar\omega} \quad (4)$$

Where $\hbar\omega$ and Φ are the photon energy and the intensity of the incident photon fluxes, respectively.

The absorption of the structure was obtained by the following equation:

$$A = 1 - T - R \quad (5)$$

T and R, are transmission and reflection parameters, sequentially.

B. Design of BP Photodetector with Circular Antenna

The antenna-assisted BP mid-IR photodetector on a silicon substrate is depicted in Fig. 1. To study the absorption features of the proposed device, the geometrical parameters are optimized. The Particle Swarm optimization algorithm is used to find the optimum thickness of BP and antenna layer on silicon. The optimum thickness is the thickness that gives the maximum absorption at the wavelength of operation, in this case $4\mu\text{m}$.

The proposed photodetector has $N=3$ rows and $M=2$ columns of Au/Pd circular antennas. These metallic antennas as electrodes in photodetectors can collect the generated photo carriers very effectively. To reduce the contact resistance among the BP layer and antennas, a thin layer made of palladium (Pd) with 10nm thickness under the gold electrodes is utilized. The circular antenna electrodes in the whole simulations are 200nm radius and 40nm thick (Pd thickness is 10nm and Au thickness is 30nm). The gate dielectric is 200nm SiO₂. The thickness and area of the BP sheet as a channel photodetector upon the top of Si/SiO₂ substrate are 12nm and $4.48\mu\text{m}^2$ respectively.

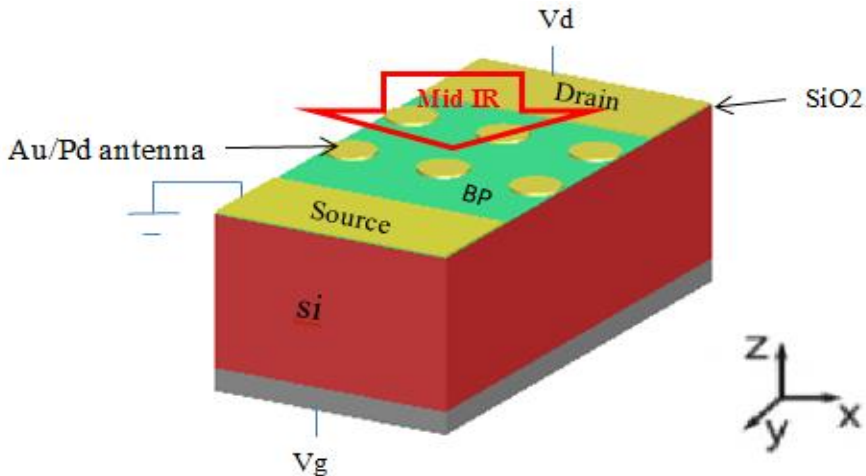


Fig. 1. 3D schematic of the antenna-assisted black phosphorus photodetector on a silicon substrate.

3. RESULTS AND DISCUSSION

A. Optical Characterization

We first performed optical characterization of BP detectors by numerical FDTD simulation. BP with a thickness of 12nm transferred onto Si substrates to determine the total generation rate. Afterward, the obtained generation rate was transported to the DEVICE module to investigate electrical characterization. Parameters of the BP layer such as bandgap, dc permittivity, etc. are mentioned in Table 1.

TABLE I

PARAMETERS AND STRUCTURAL DIMENSIONS OF BP THAT USED IN THIS SIMULATION [44, 45]

Parameter	BP
Layer thickness (nm)	12
Bandgap E_g (eV)	0.3
Dc permittivity	5
n_i (cm^{-3})	25
Work function (eV)	5.16
Electron mobility ($\text{cm}^{-2}\text{V}^{-1}\text{s}^{-1}$)	1100
Hole mobility ($\text{cm}^{-2}\text{V}^{-1}\text{s}^{-1}$)	640
SRH lifetime for e (s)	2.2×10^{-10}
SRH lifetime for h (s)	2.2×10^{-10}
Radiative lifetime for e/h (s)	2.2×10^{-14}
Interface recombination velocity (cm.s^{-1})	2.2×10^7

To evaluate the influence of antenna on absorption, the absorption under an illumination intensity of 1W.cm^{-2} and wavelength range $1-5\mu\text{m}$ has been plotted in Fig. 2. As can be seen, BP photodetector with antennas has better absorption than the device without any antennas (wavelength range: 1 to 5 μm). The absorption of antenna-assisted BP photodetector reaches 15% around $4\mu\text{m}$, which is 15 times larger than the absorption of the device without antennas. The circular antennas are applied in the role of both electrodes and light-harvesting mechanisms to concurrently increase light absorption and optical carrier collection performance.

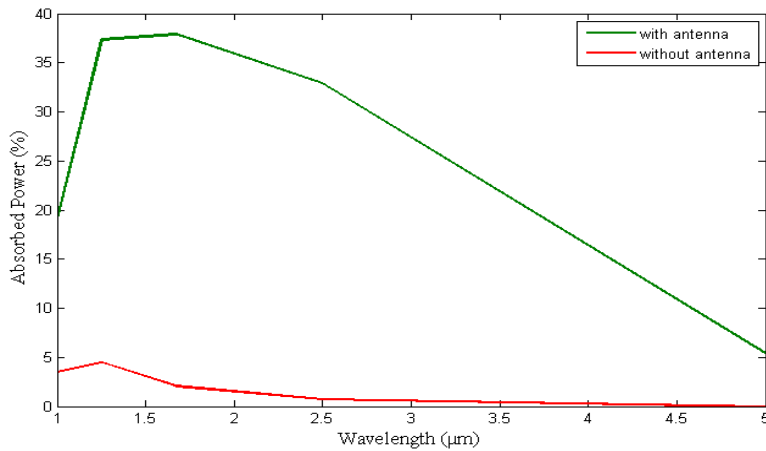


Fig. 2. Effect of metallic antennas on optical absorption of the device.

According to the FDTD simulation, the distribution of electric field intensity ($|E|^2 \cdot |E_0|^{-2}$) at $\lambda = 4\mu\text{m}$ is obtained and also depicted in Fig. 3. A monochromatic incident light beam of intensity $1\text{W}\cdot\text{cm}^{-2}$ is focused on the nanogaps among antennas (gap magnitude $\lambda = 0.4\mu\text{m}$) and duo to the Extremely High electric field intensity inward the nanogap, the light BP interaction enhanced and light absorption in BP will be increased.

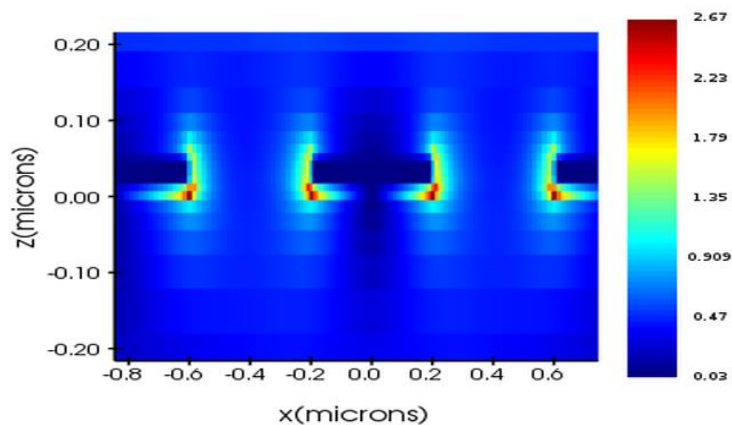


Fig. 3. Electric field intensity enhancement distribution in the xz-plane, relative to the incident plane wave.

The generation rate is averaged along the length of the structure. Then total generation rate is used as the input into the electrical stimulation. Fig. 4 displays the generation rate (g) at $z = -982nm$ and illustrations where the absorbed photons (electron-hole pairs) are concentrated. As can be seen from Fig. 4, the absorption is high at the surface of Au/Pd antennas and drops as we move to the side of the BP film.

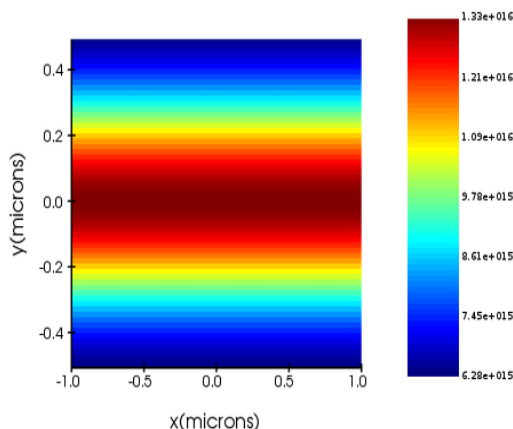


Fig. 4. The optical generation rate at $\lambda = 4\mu m$ and $z = -982nm$.

B. Electrical Characterization

The electrical characteristics of the BP photodetector with circular antennas under illuminations of different incident light energies in the mid-IR spectral region were simulated using lumercial /DEVICE. Fig. 5 shows the efficacy of the gate voltage on the drain current throughout the BP channel of the photodetector with source and drain contacts (Au/Pd), in dark and under illumination with the intensity of light incident $1W.cm^{-2}$ and wavelength= $4\mu m$. Note that the increase of the drain current with the larger applied bias voltage is due to the more efficient dissociation of photocarriers under a higher electric field.

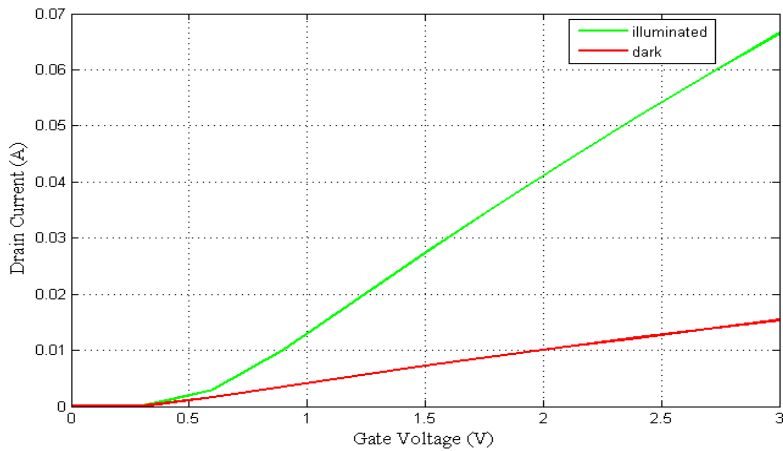


Fig. 5. Transfer characteristics of the antenna-assisted BP photodetector at a drain bias of 0.5V measured in a dark and under illumination.

Fig. 6 depicts the photocurrent I_{ph} of the photodetectors with and without circular antennas to the gate voltage (V_g) at a drain voltage $V_d = 0.5V$. The photocurrent of the proposed BP detector increases more than 5 times ($5 \times 10^{-2} A$ for $\lambda_0 = 4\mu m$ at $V_g = 3V$) compared to devices without antennas ($< 1 \times 10^{-2} A$).

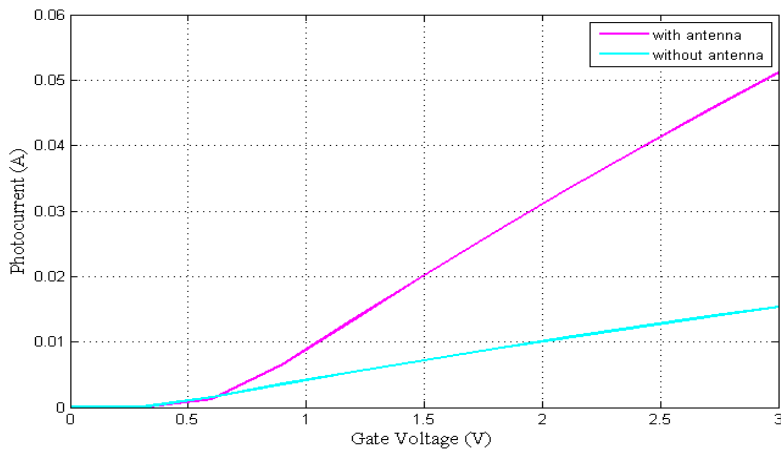


Fig. 6. Photocurrent of the BP photodetectors with and without antennas as a function of back-gate voltage. The incident wavelength is $\lambda = 4\mu\text{m}$ and the drain voltage is

$$V_d = 0.5V .$$

The variation of photocurrent to the drain-source voltage (V_{sd}) under the illumination of $\lambda = 4\mu\text{m}$ light is shown in Fig. 7. The photocurrent increases while V_{sd} changes from 0 to 3V owing to the increase of carrier drift velocity and decrease the transit time of the carrier. At this regime, it displays an n-type behavior, and the conducting channel is dominated by electrons.

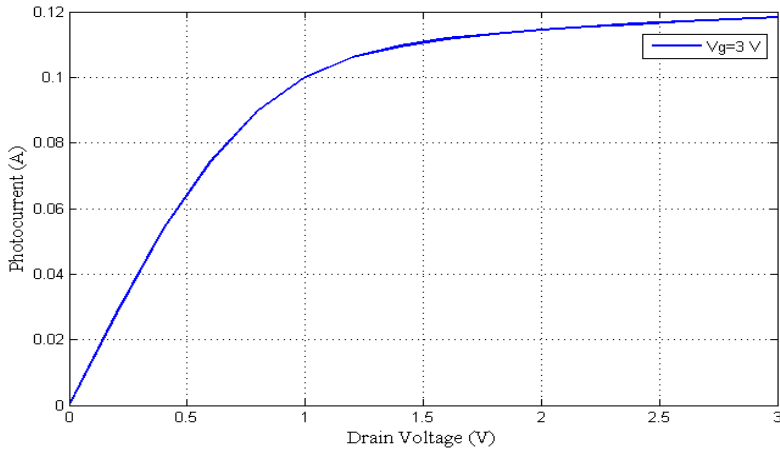


Fig. 7. Photocurrent of the BP photodetectors with antennas as a function of drain voltage. The incident wavelength is $\lambda = 4\mu\text{m}$ and the gate voltage is $V_g = 3V$

Fig. 8 displays photocurrent to the excitation power (P_{in}) with 2 V applied bias and $V_d = 0.5V$. It is found that the photocurrent gradually increases from $4.26 \times 10^{-5} A$ to $3.82 \times 10^{-2} A$ when the incident power grows from 0.0001 to 1W at $\lambda = 4\mu\text{m}$.

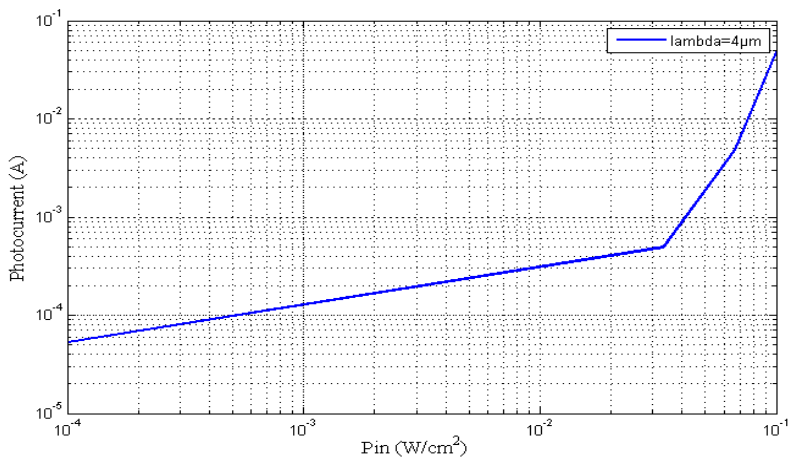


Fig. 8. Photocurrent of the device as a function of different incident laser power measured at $V_g = 2V$ and $V_d = 0.5V$.

We also calculated and plotted the responsivity to the excitation power at $\lambda = 4\mu m$, as shown in Fig.9. The responsivity decreases when the power of incident light increases as predictable from further research results [46]. We can achieve to appropriate responsivity as high as $6.25 A.W^{-1}$ at a light power of $400mWcm^{-2}$.

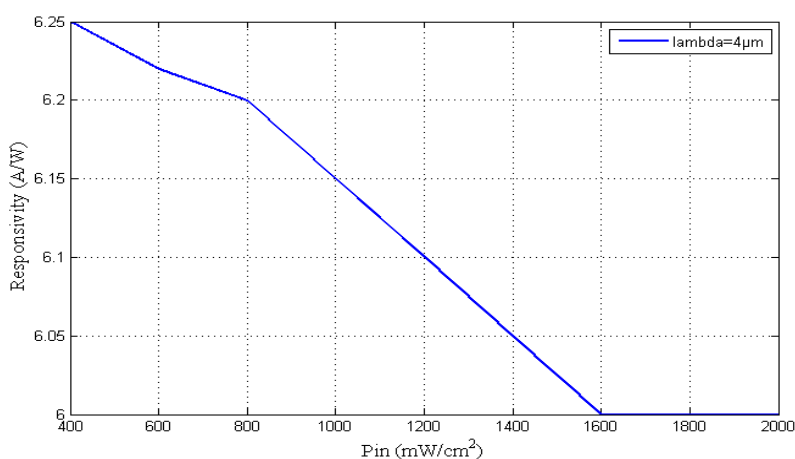


Fig. 9. The responsivity of the proposed BP photodetector to the excitation power

4. CONCLUSIONS

In this study, we have proposed mid-IR antenna-assisted BP detectors that use circular Au/Pd antennas to concurrently increase light absorption and optical carrier collection performance. Optical Characterization shows that the absorption of antenna-assisted BP photodetector reaches 15% around $4\mu m$, which is 15 times larger than the absorption of the device without antennas. We have also shown the generation rate at $z = -982nm$ and illustrated where the absorbed photons are concentrated. As a result, the absorption is high at the surface of Au/Pd antennas and drops as we move to the side of the BP film. The numerical result shows that the photocurrent of the mid-IR antenna-assisted BP detector was 5 times larger than that of the BP photodetector without antennas. Additionally, the enhanced photocurrent and responsivity of the proposed photodetector under the illumination of $4\mu m$ light with different drain voltage and incident powers were analyzed. It was found that when the light power intensity increases from 0.0001 to 1W, the photocurrent enhances at $\lambda = 4\mu m$ as predictable from further research results. through this research, we provide a good way to improve light absorption and carrier collection efficiency of mid-IR BP detectors that can play a significant role in the optoelectronic application.

REFERENCES

- [1] S. Jeon, et al., *Black phosphorus photodetector integrated with Au nanoparticles*. Appl. Phys. Lett. [Online]. 115(18) (2019, Oct) 183102. Available: <https://doi.org/10.1063/1.5119833>
- [2] B. Deng, et al., *Progress on black phosphorus photonics*. Adv. Opt. Mater. [Online] 6(19) (2018, Oct) 1800365. Available: <https://doi.org/10.1002/adom.201800365>
- [3] R. Irshad, et al., *A revival of 2D materials, phosphorene: Its application as sensors*. Ind Eng Chem. [Online] 64 (2018, Aug) 60-9. Available: <https://doi.org/10.1016/j.jiec.2018.03.010>
- [4] PC. Debnath, K. Park, YW. Song. *Recent Advances in Black- Phosphorus- Based Photonics and Optoelectronics Devices*. Small Methods. [Online] 2(4) (2018, Apr) 1700315. Available: <https://doi.org/10.1002/smt.201700315>

- [5] B. Deng, et al., *Efficient electrical control of thin-film black phosphorus bandgap*. Nat. Commun. [Online] 8(1) (2017, Apr) 1-7. Available: <https://doi.org/10.1038/ncomms14474>
- [6] N. Youngblood, M. Li. *Ultrafast photocurrent measurements of a black phosphorus photodetector*. Appl. Phys. Lett. [Online] 110(5) (2017, Jan) 051102. Available: <https://doi.org/10.1063/1.4975360>
- [7] C. Li, et al., *Tunable bandgap and optical properties of black phosphorene nanotubes*. Materials. [Online] 11(2) (2018, Feb) 304. Available: <https://doi.org/10.3390/ma11020304>
- [8] M. Akbari, R. Faez. *A Computational Study on the Performance of Graphene Nanoribbon Field Effect Transistor*. JOPN. [Online] 2(3) (2017, Aug) 1-2. Available: http://journals.miau.ac.ir/article_2427.html
- [9] L. Huang, et al., *Waveguide-integrated black phosphorus photodetector for mid-infrared applications*. ACS nano. [Online] 13(1) (2018, Dec) 913-21. Available: <https://doi.org/10.1021/acs.nano.8b08758>
- [10] M. Long, et al., *Progress, challenges, and opportunities for 2D material-based photodetectors*. Adv. Funct. Mater. [Online] 29(19) (2019, May) 1803807. Available: <https://doi.org/10.1002/adfm.201803807>
- [11] K. Cho, J. Yang, Y. Lu. *Phosphorene: An emerging 2D material*. J. Mater. Res. [Online] 32(15) (2017, Aug) 2839-47. Available: <https://doi.org/10.1557/jmr.2017.71>
- [12] L. Huang, et al., *Infrared black phosphorus phototransistor with tunable responsivity and low noise equivalent power*. ACS Appl. Mater. Interfaces. [Online] 9(41) (2017, Oct) 36130-6. Available: <https://doi.org/10.1021/acsami.7b09713>
- [13] X. Wang, S. Lan. *Optical properties of black phosphorus*. Adv. Opt. Photonics. [Online] 8(4) (2016, Dec) 618-55. Available: <https://doi.org/10.1364/AOP.8.000618>

- [14] T. Liu, et al., *Black phosphorus-based anisotropic absorption structure in the mid-infrared*. Opt. Express. [Online] 27(20) (2019, Sep) 27618-27. Available: <https://doi.org/10.1364/OE.27.027618>
- [15] X. Chen, et al., *Widely tunable black phosphorus mid-infrared photodetector*. Nat. Commun. [Online] 8(1) (2017, Nov) 1-7. Available: <https://doi.org/10.1038/s41467-017-01978-3>
- [16] M. Amani, et al., *Mid-wave infrared photoconductors based on black phosphorus-arsenic alloys*. ACS nano. [Online] 11(11) (2017, Nov) 11724-31. Available: <https://doi.org/10.1021/acsnano.7b07028>
- [17] S. Zhang, et al., *Simulation investigation of strained black phosphorus photodetector for middle infrared range*. Opt. Express. [Online] 25(20) (2017, Oct) 24705-13. Available: <https://doi.org/10.1364/OE.25.024705>
- [18] M. Mansuri, et al., *Numerical modeling of a nanostructure gas sensor based on plasmonic effect*. JOPN. [Online] 4(2) (2019, May) 29-44. Available: http://jopn.miau.ac.ir/article_3476.html
- [19] Q. Guo, et al., *Black phosphorus mid-infrared photodetectors with high gain*. Nano Lett. [Online] 16(7) (2016, Jul) 4648-55. Available: <https://doi.org/10.1021/acs.nanolett.6b01977>
- [20] M. Xu, et al., *Black phosphorus mid-infrared photodetectors*. Appl. Phys. B. [Online] 123(4) (2017, Apr) 130. Available: <https://doi.org/10.1007/s00340-017-6698-7>
- [21] TY. Chang, et al., *Ultra-broadband, high speed, and high-quantum-efficiency photodetectors based on black phosphorus*. ACS Appl. Mater. Interfaces. [Online] 12(1) (2019, Dec) 1201-9. Available: <https://doi.org/10.1021/acsmi.9b13472>
- [22] X. Zong, et al., *Black phosphorus-based van der Waals heterostructures for mid-infrared light-emission applications*. Light Sci. Appl. [Online] 9(1) (2020, Jul) 1-8. Available: <https://doi.org/10.1038/s41377-020-00356-x>
- [23] L. Ye, et al., *Highly polarization sensitive infrared photodetector based on*

- black phosphorus-on-WSe2 photogate vertical heterostructure*. Nano Energy. [Online] 37(2017, Jul) 53-60. Available: <https://doi.org/10.1016/j.nanoen.2017.05.004>
- [24] Y. Liu, et al., *Highly responsive broadband black phosphorus photodetectors*. Chin. Opt. Lett. [Online] 16(2) (2018, Feb) 020002. Available: <https://www.osapublishing.org/col/abstract.cfm?URI=col-16-2-020002>
- [25] J. Wu, et al., *Colossal ultraviolet photoresponsivity of few-layer black phosphorus*. ACS nano. [Online] 9(8) (2015, Aug) 8070-7. Available: <https://doi.org/10.1021/acs.nano.5b01922>
- [26] M. Huang, et al., *Broadband black-phosphorus photodetectors with high responsivity*. Adv. Mater. [Online] 28(18) (2016, May) 3481-5. Available: <https://doi.org/10.1002/adma.201506352>
- [27] R. Kochar, S. Choudhary. *MoS₂/phosphorene heterostructure for optical absorption in visible region*. IEEE J. Quantum Electron. [Online] 54(4) (2018, Jun) 1-6. Available: [10.1109/JQE.2018.2850450](https://doi.org/10.1109/JQE.2018.2850450).
- [28] YM. Qing, HF. Ma, TJ. Cui. *Tailoring anisotropic perfect absorption in monolayer black phosphorus by critical coupling at terahertz frequencies*. Opt. Express. [Online] 26(25) (2018, Dec) 32442-50. Available: <https://doi.org/10.1364/OE.26.032442>
- [29] D. Dong, et al., *Designing a nearly perfect infrared absorber in monolayer black phosphorus*. Appl. Opt. [Online] 58(14) (2019, May) 3862-9. Available: <https://doi.org/10.1364/AO.58.003862>
- [30] T. Liu, et al., *Black phosphorus-based anisotropic absorption structure in the mid-infrared*. Opt. Express. [Online] 27(20) (2019, Sep) 27618-27. Available: <https://doi.org/10.1364/OE.27.027618>
- [31] R. Audhkhiasi, ML. Povinelli. *Gold-black phosphorus nanostructured absorbers for efficient light trapping in the mid-infrared*. Opt. Express. [Online] 28(13) (2020, Jun) 19562-70. Available: <https://doi.org/10.1364/OE.398641>

- [32] N. Sefidmooye Azar, et al., *Long-Wave Infrared Photodetectors Based on 2D Platinum Diselenide atop Optical Cavity Substrates*. ACS nano. [Online] 15(4) (2021, Mar) 6573-81. Available: <https://doi.org/10.1021/acsnano.0c09739>
- [33] CH. Liu, et al., *Graphene photodetectors with ultra-broadband and high responsivity at room temperature*. Nat. Nanotechnol. [Online] 9(4) (2014, Apr) 273-8. Available: <https://doi.org/10.1038/nnano.2014.31>
- [34] S. Salimpour, H. Rasooli. *Impressive reduction of dark current in InSb infrared photodetector to achieve high temperature performance*. JOPN. [Online] (2018, Oct) 3(4) 81-96. Available: http://jopn.miau.ac.ir/article_3265.html
- [35] M. Hasani, R. Chegell. *Electronic and Optical Properties of the Graphene and Boron Nitride Nanoribbons in Presence of the Electric Field*. JOPN. [Online] 5(2) (2020, May) 49-64. Available: http://jopn.miau.ac.ir/article_4218.html
- [36] Y. Yao, et al., *High-responsivity mid-infrared graphene detectors with antenna-enhanced photocarrier generation and collection*. Nano Lett. [Online] 14(7) (2014, Jul 9) 3749-54. Available: <https://doi.org/10.1021/nl500602n>
- [37] M. Riaz, et al., *Computer analysis of microcrystalline silicon hetero-junction solar cell with numerical FDTD/DEVICE*. Int. J. Comput. Mater. Sci. Eng. [Online] 6(03) (2017, Sep) 1750017. Available: <https://doi.org/10.1142/S2047684117500178>
- [38] S. Jalaei, J. Karamdel, H. Ghalami-Bavil-Olyae. *Mid- Infrared Photodetector Based on Selenium- Doped Black Phosphorus*. Phys. Status Solidi A. [Online] 217(23) (2020, Dec) 2000483. Available: <https://doi.org/10.1002/pssa.202000483>
- [39] F. Ostovari, MK. Moravvej-Farshi. *Photodetectors with armchair graphene nanoribbons and asymmetric source and drain contacts*. Appl. Surf. Sci.

- [Online] 318 (2014, Nov) 108-12. Available: <https://doi.org/10.1016/j.apsusc.2014.01.117>
- [40] AN. Rudenko, S. Yuan, MI. Katsnelson. *Toward a realistic description of multilayer black phosphorus: From g w approximation to large-scale tight-binding simulations*. Phys. Rev. B. [Online] 92(8) (2015, Aug) 085419. Available: <https://doi.org/10.1103/PhysRevB.92.085419>
- [41] S. Datta. *Nanoscale device modeling: the green's function method*. Superlattices Microstruct. [Online] 28(4) (2000, Oct) 253-78. Available: <https://doi.org/10.1006/spmi.2000.0920>
- [42] M. Zavvari, Y.Zehforoosh. *Study of Photo-Conductivity in MoS₂ Thin Films Grown in Low-Temperature Aqueous Solution Bath*. JOPN. [Online] 4(4) (2019, Dec) 53-64. Available: http://jopn.miau.ac.ir/article_3760
- [43] M. Long, et al., *Room temperature high-detectivity mid-infrared photodetectors based on black arsenic phosphorus*. Sci. Adv. [Online] 3(6) (2017, Jun) 1700589. Available: <https://doi.org/10.1126/sciadv.1700589>
- [44] Y. Cai, G. Zhang, YW. Zhang. *Layer-dependent band alignment and work function of few-layer phosphorene*. Sci. Rep. [Online] 4(1) (2014, Oct) 1-6. Available: <https://doi.org/10.1038/srep06677>
- [45] Z. Nie, et al., *Ultrafast photocarrier recombination dynamics in black phosphorus-molybdenum disulfide (BP/MoS₂) heterostructure*. arXiv preprint arXiv. [Online] 1811.04706. (2018, Nov) Available: <https://arxiv.org/abs/1811.04706>.
- [46] L. Huang, et al., *Infrared black phosphorus phototransistor with tunable responsivity and low noise equivalent power*. ACS Appl. Mater. Interfaces. [Online] 9(41) (2017, Oct) 36130-6. Available: <https://doi.org/10.1021/acsami.7b09713>

